Ultrasound controlled mechanophore activation in hydrogels for cancer therapy

Gun Kim[a,b,c,1], Qiong Wu[a,d,e,1], James L. Chu[a,b], Emily J. Smith[a,b], Michael L. Oelze[a,b,f,g], Jeffrey S. Moore[a,b,d,e,2], and King C. Li[a,b,g,2]

[a]Beckman Institute for Advanced Science and Technology, University of Illinois at Urbana–Champaign, Urbana, IL 61801; [b]Carle Illinois College of Medicine, University of Illinois at Urbana Urbana–Champaign, Urbana, IL 61820; [c]Department of Urban and Environmental Engineering, Ulsan National Institute of Science and Technology, Ulsan 44919, Republic of Korea; [d]Department of Chemistry, University of Illinois at Urbana–Champaign, Urbana, IL 61801; [e]Department of Materials Science and Engineering, University of Illinois at Urbana–Champaign, Urbana, IL 61801; [f]Department of Electrical and Computer Engineering, University of Illinois at Urbana–Champaign, Urbana, IL 61801; and [g]Department of Bioengineering, University of Illinois at Urbana–Champaign, Urbana, IL 61801

Contributed by Jeffrey S. Moore; received May 26, 2021; accepted December 9, 2021; reviewed by Andrew Boydston, Kim Butts Pauly, and Yan Xia

Mechanophores are molecular motifs that respond to mechanical perturbance with targeted chemical reactions toward desirable changes in material properties. A large variety of mechanophores have been investigated, with applications focusing on functional materials, such as strain/stress sensors, nanolithography, and self-healing polymers, among others. The responses of engineered mechanophores, such as light emittance, change in fluorescence, and generation of free radicals (FRs), have potential for bioimaging and therapy. However, the biomedical applications of mechanophores are not well explored. Herein, we report an in vitro demonstration of an FR-generating mechanophore embedded in biocompatible hydrogels for noninvasive cancer therapy. Controlled by high-intensity focused ultrasound (HIFU), a clinically proven therapeutic technique, mechanophores were activated with spatiotemporal precision to generate FRs that converted to reactive oxygen species (ROS) to effectively kill tumor cells. The mechanophore hydrogels exhibited no cytotoxicity under physiological conditions. Upon activation with HIFU sonication, the therapeutic efficacies in killing in vitro murine melanoma and breast cancer tumor cells were comparable with lethal doses of H_2O_2. This process demonstrated the potential for mechanophore-integrated HIFU combination as a noninvasive cancer treatment platform, named "mechanochemical dynamic therapy" (MDT). MDT has two distinct advantages over other noninvasive cancer treatments, such as photodynamic therapy (PDT) and sonodynamic therapy (SDT). 1) MDT is ultrasound based, with larger penetration depth than PDT. 2) MDT does not rely on sonosensitizers or the acoustic cavitation effect, both of which are necessary for SDT. Taking advantage of the strengths of mechanophores and HIFU, MDT can provide noninvasive treatments for diverse cancer types.

mechanochemistry | hydrogel | ultrasound | reactive oxygen species | cancer therapy

When mechanical force is applied to polymers, the mechanical energy is transiently accumulated along their chain-like backbones. At sufficient energy levels, covalent bonds in the polymer chain break to induce chemical reactions, a process known as polymer mechanochemistry (1). Conventionally, polymer mechanochemistry was considered destructive because chain scission resulted in lower molecular weight and reduction in mechanical properties. However, by strategically embedding a weak bond in the polymer chain, selective bond scission triggers desirable, constructive chemical reactions (1). Various force-responsive molecular motifs, known as mechanophores, were successfully designed, resulting in mechanoresponsive materials (1). Under mechanical perturbation, mechanophores can exhibit color change (2); fluorescence turn on (3, 4); light emission (5); polymer backbone alteration (6); and the generation of acid (7), catalysts (8, 9), small molecules (10), or free radicals (FRs) (11). These property changes have been demonstrated for various applications, such as stress sensing (12–14), damage detection (15, 16), surface patterning (17), self-healing/strengthening (18–20), nanolithography (17), etc. Although most studies have been focusing on functional materials, mechanophores also have potential in biomedical applications (21). For example, activation of dioxetane mechanophores results in the emission of blue light at a wavelength of ∼470 nm, which is suitable for optogenetic applications (e.g., optotriggering of muscle cells) (5). The activation of azo mechanophores produces FRs (11), which are key components for existing cancer therapies, such as type I photodynamic therapy (PDT) and radiotherapy (22). However, the biomedical applications of mechanophores are yet to be well explored, which is mainly due to the lack of a triggering system capable of targeted delivery of mechanical energy.

Therapeutic ultrasound offers the potential for spatiotemporally controlled activation of mechanophores under physiological conditions. Therapeutic ultrasound is noninvasive and spatiotemporally precise with clinically relevant penetration depth. Sonodynamic therapy (SDT) is one of the most

Significance

Biomedical application of mechanophores is the next frontier in polymer mechanochemistry. We report the concept, mechanochemical dynamic therapy (MDT), that utilizes remote, ultrasound-triggered mechanophore activation to enable anticancer activities. We selected an azo-based mechanophore to generate reactive free radicals (FRs) under the control of high-intensity focused ultrasound (HIFU), which subsequently produced ROS. We investigated two sets of in vitro mouse cancer models: 1) melanoma (B16F10) and 2) breast cancer (E0771). Inhibition of growth and decreases in viabilities of both B16F10 and E0771 were observed in correlation to the release of ROS by mechanophore activation. By circumventing the known issues in photodynamic therapy and sonodynamic therapy, we anticipate MDT to be a powerful anticancer tool complementary to other existing cancer treatments.

Author contributions: G.K., Q.W., M.L.O., J.S.M., and K.C.L. designed research; G.K., Q.W., and J.L.C. performed research; G.K., Q.W., E.J.S., and M.L.O. analyzed data; M.L.O., J.S.M., and K.C.L. supervised the study; and G.K., Q.W., J.L.C., and M.L.O. wrote the paper.

Reviewers: A.B., University of Wisconsin–Madison; K.B.P., Stanford University; and Y.X., Stanford University.

The authors declare no competing interest.

[1]G.K. and Q.W. contributed equally to this work.

[2]To whom correspondence may be addressed. Email: jsmoore@illinois.edu or kingli@illinois.edu.

This article contains supporting information online at http://www.pnas.org/lookup/suppl/doi:10.1073/pnas.2109791119/-/DCSupplemental.

Published January 19, 2022.

promising applications of therapeutic ultrasound currently in development (23). The concept of SDT is derived from PDT, a clinically proven noninvasive cancer treatment. In general, PDT requires light, oxygen, and photosensitizers that harvest photoenergy (24). The harvested photoenergy is transferred to tissue oxygen to produce therapeutic reactive oxygen species (ROS) that kill the tumor cells (25, 26). Despite promising outcomes for clinical translation, however, the methodology of PDT has inherent shortcomings. Poor tissue penetrance of light is one of the main limitations, making PDT unsuitable for deep-seated tumors in the absence of invasive optic fiber implants. In contrast, ultrasound penetrates intervening tissues and delivers acoustic energy noninvasively to deep areas of the body (27). Studies have found that ultrasonic cavitation energy can be harvested by some photosensitizers used in PDT (28–32) to generate ROS and potentiate tumor killing in animal models. This synergistic effect overcomes the tissue penetration limit of PDT while remaining minimally invasive, leading to a high therapeutic potential of SDT, particularly for deep tumors (23). However, current SDT methods rely on the ultrasonic cavitation effect (33, 34), which inherently limits the spatiotemporal precision of ultrasonic energy delivery. Furthermore, in most SDT applications, microbubble injections are also required for the cavitation effect, adding to the complexity of in vivo or clinical applications (34). Another clinical application of therapeutic ultrasound is targeted drug release (35–37). Under the remotely deposited ultrasonic energy, polymeric micelle carriers are triggered to release drugs for intracellular uptake. The kinetics and cytotoxic effect of ultrasound-triggered drug release have been thoroughly studied and demonstrated to be feasible for potential clinical applications. However, this method again relies on the acoustic cavitation effect to destroy the micellar structure for drug release. Therefore, developing a new therapeutic technology that does not relying on cavitation is necessary to take full advantage of the spatiotemporal precision offered by therapeutic ultrasound.

Recently, we demonstrated that high-intensity focused ultrasound (HIFU), a clinically validated noninvasive therapeutic ultrasound, enables mechanophore activation in synthetic polymeric materials without relying on the cavitation effect, suggesting possible directions for the clinical use of mechanophores (e.g., optotriggering cells using the mechanophore-induced blue light) (38). We further demonstrated ∼86% efficiency in HIFU-induced mechanophore activation through a rodent skull–embedded polymer, suggesting feasibility for potential in vivo transcranial applications (38). Herein, we introduce a role of mechanophores as a therapeutic agent capable of targeted release of ROS under the control of HIFU triggering, which provides advantages over the above-mentioned issues in current ultrasonic modalities: a cavitation-free effect that does not need microbubbles and that is capable of more efficient spatiotemporal control of ultrasonic energy. To achieve this, we selected azo-based mechanophores covalently embedded in cross-linked biocompatible polyethylene glycol (PEG) hydrogels. We then developed an HIFU setup that delivers spatiotemporally controlled radiation force to acoustically activate the azo-based mechanophores. ROS generation is validated via luminol chemiluminescence and colorimetric tests. Finally, we investigate the cytotoxic effect of the mechanophore-induced ROS using in vitro mouse melanoma (B16F10) and breast cancer (E0771) models. We observed ∼100% death rate of the two types of tumor cells over 72 h after HIFU triggering of mechanophore hydrogel while observing no cytotoxicity in the absence of the HIFU treatment. These results suggest that targeted release of ROS, by biomedically tuned mechanophores under HIFU, holds great potential as a platform for cancer treatment, termed "mechanochemical dynamic therapy" (MDT). Furthermore, we hypothesize that MDT can operate synergistically with other current forms of cancer treatment and is highly compatible with medical imaging techniques (e.g., magnetic resonance imaging [MRI], quantitative ultrasound, etc.), providing direct evidence on the therapeutic efficacy of MDT.

Results and Discussion

Synthesis and Cytotoxicity Study of Azo Mechanophore-Embedded PEG Hydrogels. The concept of MDT is outlined in Fig. 1. PEG hydrogels embedded with azo mechanophores were synthesized from azo-PEG copolymer macroinitiator and PEG diacrylate cross-linker (*SI Appendix*, *SI Materials and Methods*). Upon curing at high temperature, ∼14% of the azo groups thermally decomposed into FRs (Fig. 2*A* and *SI Appendix*, Table S1), allowing the addition of the cross-linker into the hydrogel networks (*SI Appendix*, Fig. S1). The majority (∼86%) of azo groups did not thermally decompose and thus, were incorporated into the hydrogel network as mechanophores for on-demand FR generation (Fig. 2*A* and *SI Appendix*, Fig. S2). This synthetic strategy avoids the use of toxic chemicals and is potentially suitable for scalable, low-cost production. As a control, hydrogels without mechanophores were prepared similarly by polymerizing the PEG diacrylate cross-linkers with a small molecular azo initiator, the potassium salt of 4,4'-azobis (4-cyanovaleric acid) (ACVA). Afterward, unreacted ACVA was removed during purification. As evidence that MDT is a mechanical rather than thermal effect, we determined that the azo mechanophores exhibit good thermal stability, with a very low (∼2%/d) background decomposition rate at the physiological temperature of 37 °C (Fig. 3*A* and *SI Appendix*, Table S1). Moreover, thermally decomposed azo mechanophores are unlikely to generate reactive FRs, given the propensity of thermally induced FR pairs to recombine into nontoxic products (11). In contrast, mechanically generated FR pairs do not recombine because they are pulled apart upon generation (10). As expected, the nonactivated mechanophore hydrogels demonstrated no in vitro cytotoxicity under physiological conditions over at least 72 h (Fig. 3*B*) for both mouse melanoma and breast cancer cells. The azo mechanophores were also stable for long-term storage (decomposition: <2%/y at 4 °C) and capable of temporary ambient storage (decomposition: ∼0.3%/d at 25 °C).

Mechanical Activation of Azo Mechanophore Using HIFU and Detection of ROS. An HIFU-based triggering system was developed to remotely control the activation of azo mechanophores (Fig. 2*B* and *SI Appendix*, Fig. S3). For the irradiation, continuous-wave (CW) ultrasound at a frequency of 550 kHz was employed with a fixed sonication period (10 s on, 20 s off; four repetitions per spot) and a spatial-peak temporal average intensity (I_{SPTA}) of

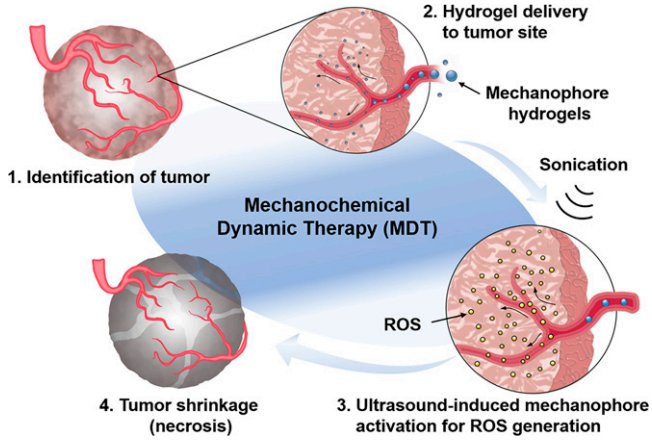

Fig. 1. The concept of MDT. Focused ultrasound controls ROS generation from mechanochemical reactions for noninvasive cancer therapy.

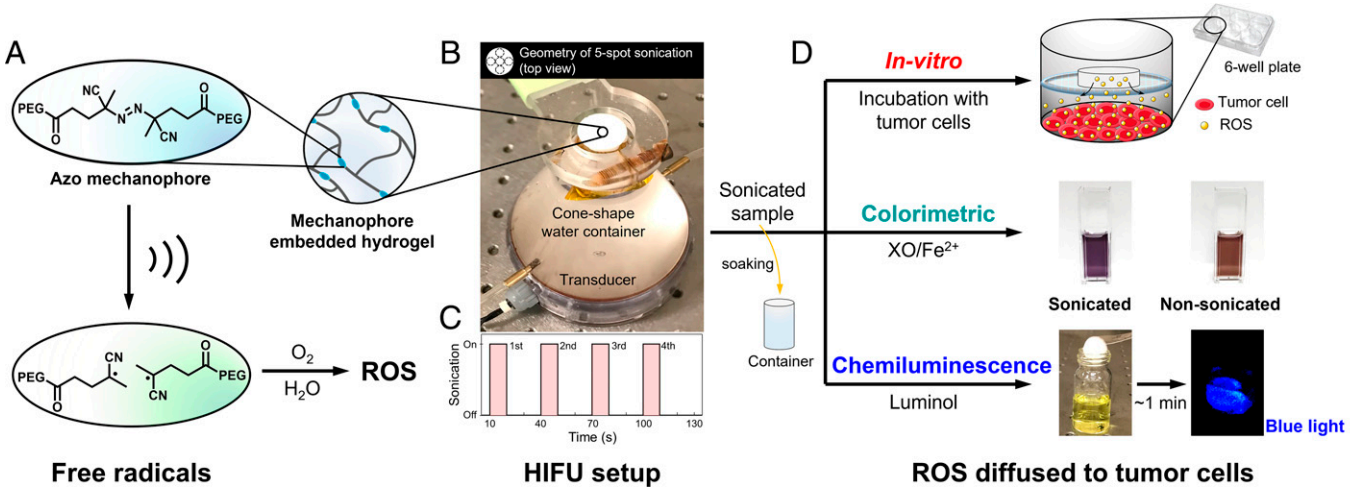

Fig. 2. (*A*) The structure of the azo-based mechanophore hydrogel for the generation of FRs and ROS under sonication. (*B*) The sonication setup. (*C*) The sonication cycles (four repetitions for each spot). (*D*) The detection of ROS and in vitro treatment.

the ultrasonic beam (115 W·cm^{-2}, ~1.9 MPa of peak acoustic pressure amplitude). The focal spot where the ultrasonic beams were located inside the mechanophore hydrogels is shown in Fig. 2*B*. The lateral location of focal spots was shifted five times to guarantee high efficiency of azo mechanophore activation. Because the azo mechanophores are responsive to both mechanical forces and heat, we first examined local heating around the focal region induced by the irradiation of mechanophore hydrogel with HIFU. The results of this experiment distinguish a mechanical from a thermal activation stimulus. We have previously validated the high efficiency of CW ultrasound on spatiotemporal control of mechanical energy delivery for mechanophore activation (e.g., color change and light emission), while the thermal effect on mechanophore activation was insignificant (38). To further understand this, we monitored the temperature elevation due to the designed HIFU sonication using both a thermal infrared camera (FLIR SC620) and a thermocouple (*SI Appendix*, Fig. S4). During HIFU operation at the selected intensity and period, the surface temperature of mechanophore hydrogels was monitored with the thermal infrared camera, and the internal temperature elevation around the focal spot was tracked with a thermocouple. We observed a temperature gradient along the depth (i.e., an averaged peak temperature of ~41.5 °C ± 0.3 °C was recorded on the surface, while the temperature recorded at the focal spot was ~53.1 °C ± 3.1 °C), suggesting that the transmitted ultrasonic energy required for the mechanophore activation was well localized at the focal spot. Furthermore, according to the thermal decomposition kinetics shown in Fig. 3*A*, while temperature elevation greater than 53 °C by CW HIFU sonication does thermally activate mechanophores within the focal spot, the decomposition percentage is less than 0.01%, combining for a mere total of <0.2% decomposition over the full five-spot sonication regime (*SI Appendix*, Fig. S4). Therefore, these results confirmed that the thermal effect was negligible and that the azo mechanophore activation was triggered by mechanical force (i.e., an acoustic radiation force) (39). We then examined the ability of the HIFU setup to generate FRs via azo mechanophore activation. Mechanophore hydrogels were subjected to five different sonication spots with fixed intensity (115 W·cm^{-2}) and four cycles, as shown in Fig. 2. We verified that the designed HIFU conditions provided a strong effect for activating azo mechanophores, facilitating the generation of FRs.

Distinct from thermally generated FRs, mechanically generated FRs were rapidly separated to prevent recombination (11). Therefore, these mechano-FRs are efficiently converted into various types of ROS, including H_2O_2 (40, 41). To validate

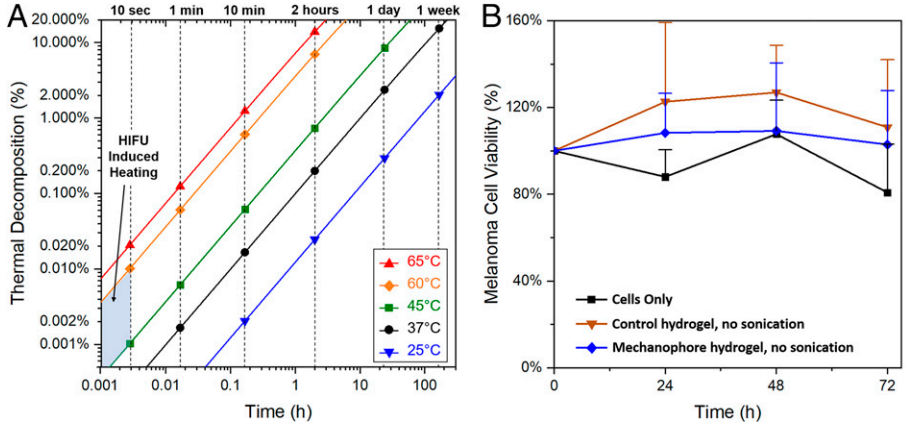

Fig. 3. (*A*) Thermal decomposition rate of the azo mechanophore calculated from the kinetics data of the azo-PEG macroinitiator. (*B*) Cytotoxicity evaluation of mechanophore and control hydrogels without sonication for melanoma cells ($n \geq 4$) and breast cancer cells ($n \geq 6$) under physiological conditions (37 °C, pH 7.4, 5% CO_2/95% O_2).

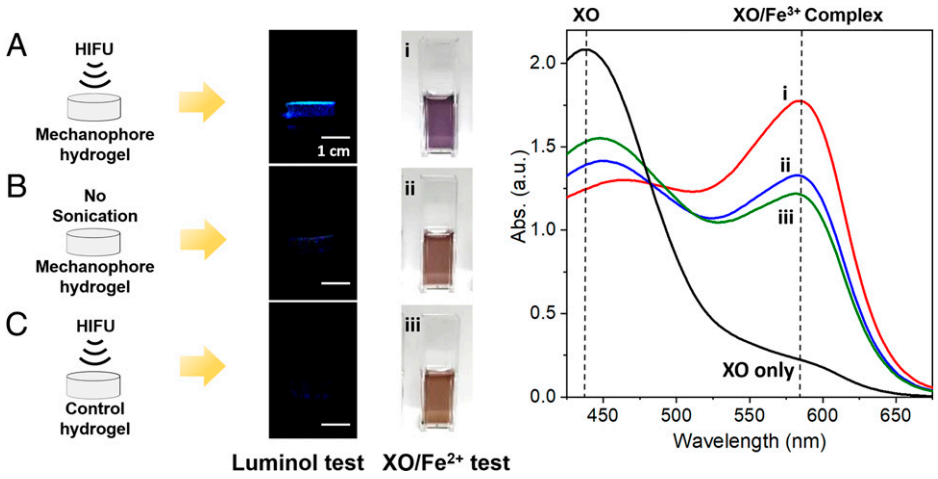

Fig. 4. Luminol chemiluminescence and XO/Fe^{2+} colorimetric tests for (*A*) sonicated mechanophore hydrogels, (*B*) mechanophore hydrogels without sonication, and (*C*) sonicated control hydrogels. Ultraviolet-visible (UV-Vis) colorimetric analysis was taken after immersing samples in XO/Fe^{2+} for 30 min for (*i*) sonicated mecheanophore hydrogels, (*ii*) mechanophore hydrogels, (*iii*) soncated control hydrogels and compared with the XO only control (no hydrogel). Abs. (a.u.), absorption (arbitrary unit).

the formation of ROS, luminol chemiluminescence and xylenol orange (XO)/Fe^{2+} colorimetric tests were performed, as shown in Figs. 2*D* and 4. During luminol tests, blue chemiluminescence was clearly observed for sonicated mechanophore hydrogels, lasting for at least several minutes (Fig. 4*A* and Movie S1), which confirmed the formation of ROS that oxidize luminol for light emission. In contrast, light emission was barely observable in control studies (Fig. 4 *B* and *C*). The colorimetric study was based on the oxidation of Fe^{2+} into Fe^{3+} that forms a purple complex with XO (41). The sonicated mechanophore hydrogel resulted in a faster color change (<30 min) than control materials (Fig. 4). However, Fe^{2+} is not selective for ROS; under prolonged reaction time, Fe^{2+} ions were oxidized by other oxidants, such as thermally stable peroxides formed during hydrogel synthesis that remained covalently bound to the polymer network (*SI Appendix*, Fig. S2) (42, 43). These stable peroxides did not impart cytotoxicity and were not active for MDT treatment, but their presence did affect the ROS quantification in this colorimetric assay.

Cytotoxicity of Mouse Cancer Cells by MDT: Melanoma (B16F10). To examine the therapeutic potential of the azo mechanophores for ROS generation, we performed in vitro challenge assays in the B16F10 murine skin melanoma cancer model. B16F10 is an aggressive metastatic form of mouse skin melanoma widely used in cancer studies. For MDT, the mechanophore hydrogels were activated and exposed to the cancer cells for 72 h via the established CW HIFU sonication procedure. The number of sonication spots (five spots) was determined after the validation of the therapeutic efficacy of ROS on cytotoxicity (*SI Appendix*, Fig. S8). Upon exposure to activated hydrogels, the viable B16F10 cell population positive for Calcein-acetoxymethyl ester (AM) fluorescence decreased over the course of 72 h in a sonication spot number–dependent manner. The number of live cells that exhibit Calcein-AM fluorescence were counted every 24 h using the FIJI software as detailed in *SI Appendix*. As shown in Fig. 5*A*, the number of live B16F10 tumor cells decreased significantly over 72 h after MDT, with the death rate close to 100% (Fig. 5*B*). In comparison, neither sonicated nonmechanophore hydrogels nor nonsonicated mechanophore hydrogels imparted statistically significant influence on the melanoma cell population over 72 h, demonstrating that both mechanophore and sonication are necessary for MDT. The overall effectiveness of MDT was comparable with the positive control experiment—a challenge by a lethal dosage of H_2O_2 of ∼50 μM (*SI Appendix*, Fig. S5)—demonstrating the potency of cell killing from ROS generation by the activated mechanophores. As an estimation, complete conversion of all azo mechanophores within the focal spots would produce ∼500 μM H_2O_2. (The estimation is based on 100% conversion of all azo moieties in the focal spots regardless of if these azo groups are capable of mechanochemical activation. The volume of each focal spot is ∼0.012 cm^3.) Therefore, ∼10% of the azo mechanophores were effectively activated during MDT.

Cytotoxicity of Mouse Cancer Cells by MDT: Breast Cancer Model (E0771). In addition to B16F10, we tested the therapeutic potential of the azo mechanophores in the E0771 murine breast cancer cell line in vitro. E0771 is a well-studied mouse breast cancer model that is strongly proliferative, aggressive, and highly metastatic. Mechanophore hydrogels were activated via the established CW HIFU sonication procedure. Upon exposure to the activated hydrogels, viable E0771 cells positive for Calcein-AM fluorescence were counted every 24 h for 72 h. As shown in Fig. 5*C*, the population of E0771 tumor cells decreased significantly over 72 h, while untreated control cells proliferated over 400%. The death rate of the MDT-treated cells was close to 100% (Fig. 5*D*). For sonicated nonmechanophore control hydrogels, modest reduction of cell proliferation was observed; however, the amount of tumor cells did not decrease significantly, and the inhibition was not sufficient for effective treatment. In the absence of mechanophores, ultrasound can still break the conventional covalent bonds in the polymer backbone of the hydrogels, which also generates FRs and ROS. Compared with activating a mechanophore, however, breaking conventional covalent bonds requires much higher mechanical force. Therefore, the amounts of ROS formed by nonmechanophore hydrogels were much lower. The ROS generated from nonmechanophore may account for the slight inhibitory effect observed from the sonicated nonmechanophore hydrogels, which is insufficient for effective cancer treatment. On the other hand, nonsonicated mechanophore hydrogels resulted in cell death counts that were not statistically significant, which was consistent with the noncytotoxicity of nonactivated mechanophore hydrogels. The overall MDT effectiveness was comparable with the positive control—challenge by lethal dosage of H_2O_2 of ∼30 μM (*SI Appendix*, Fig. S5)—again demonstrating the potency of the ROS generated by the activated mechanophores.

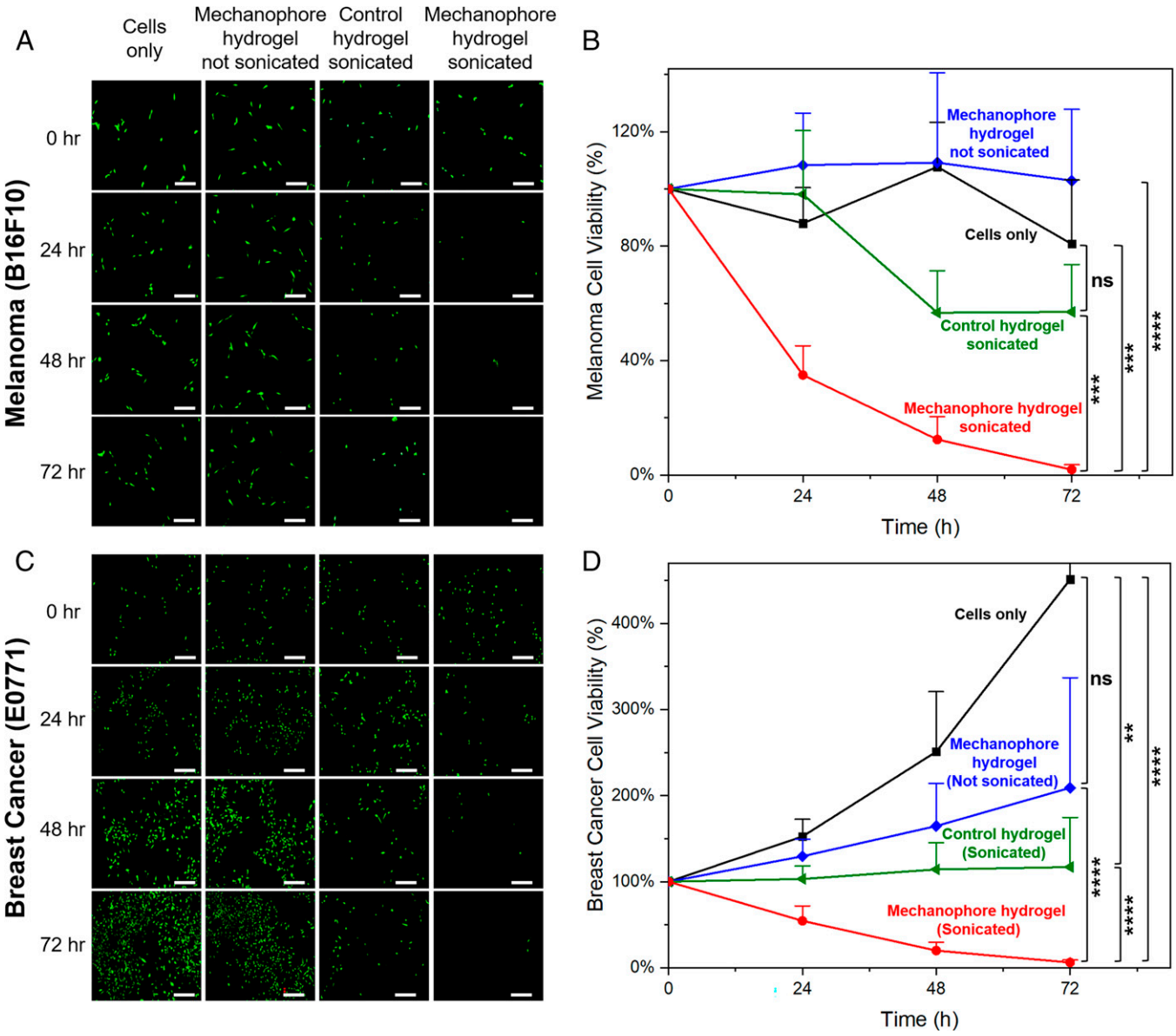

Fig. 5. Fluorescence images and quantification of live tumor cells before (0 h) and after (24 to 72 h) MDT (sonicated control and mechanophore hydrogel) compared with controls (cells only and nonsonicated mechanophore hydrogel) for melanoma (*A* and *B*) and breast cancer (*C* and *D*). Statistics were performed with *F* test, $^{**}P \leq 0.01$, $^{***}P \leq 0.001$, $^{***}P \leq 0.0001$; ns, statistically nonsignificant. (Scale bars: 250 μm.)

Conclusion

In summary, we provided a demonstration that ROS-generating mechanophores in hydrogels are of interest in a biomedical context, particularly having potential for noninvasive cancer therapy. Using azo mechanophores in a biocompatible PEG hydrogel coupled with HIFU, we developed a cancer therapy platform, MDT, enabling the targeted release of ROS. The nonactivated azo mechanophore hydrogels resulted in no cytotoxicity due to good thermostability, while upon HIFU sonication, they rapidly generate reactive FRs and ROS to kill tumor cells in a noninvasive manner. With these advances, MDT achieves therapeutic efficacy of ~100% within 72 h in in vitro tumor models, including melanoma (B16F10) and breast cancer models (E0771), which is comparable with a lethal dosage (30 to 50 μM) of H_2O_2. As a control, HIFU sonication of hydrogels without mechanophores produced limited amounts of ROS and was ineffective for effective treatment. Furthermore, evidence was provided to show the role of mechanophores in MDT with the formation of ROS. Therefore, biocompatible hydrogels embedded with azo mechanophores are promising as members of the therapeutic biomaterial family. In the present work, we focus on in vitro validation of the therapeutic efficacy of MDT, but it is worthwhile to note that conditions for HIFU sonication (e.g., intensity, penetration depth, etc.) and azo mechanophore activation (e.g., bond cleavage threshold, etc.) are tunable to meet the need of future studies. In future in vivo studies, the MDT aspect will be synergistic to the direct therapeutic effects of focused ultrasound on tumor cells. We envision that the proposed MDT method holds promise for future in vivo models and clinical applications, including nonsuperficial glioblastoma, pancreatic cancer, etc. Specifically, we are currently developing two concepts: 1) direct intratumoral injection of biocompatible hydrogels where azo mechanophores are embedded and 2) systematic injection of tumor-homing mechanophore-loaded nanocarriers. After successful development of both candidates, remote triggering of mechanophores via image-guided HIFU will facilitate

spatiotemporally precise release of ROS at the tumor site. We believe that these approaches will not only provide insights into target drug delivery via mechanical triggering of mechanophores but also, open the door for exploiting polymer mechanochemistry for clinical purposes. Together with existing imaging modalities, like ultrasound and MRI, for image guidance, MDT will provide a framework for cancer therapy.

Materials and Methods

Preparation of Azo Mechanophore PEG Hydrogels and Control Hydrogels. PEG hydrogels with azo mechanophores are synthesized using an azo-PEG macroinitiator with PEG diacrylate cross-linker (*SI Appendix*, Fig. S1). In a 40-mL vial, 3.2 g of macroinitiator and 4.8 g of PEG diacrylate were dissolved in 24 mL phosphate buffer saline (PBS; pH = 7.4) under vigorous agitation by a vortex mixer. The solution was transferred to a six-well cell-culturing plate (well area 9.6 cm^2) at a volume of 5 mL per well. The plate was sealed and heated by an oven at 65 °C for 2 h to cure the hydrogel. After cooling down, the hydrogels were cut into cylindrical samples with diameters of 1.6 cm and thicknesses of ∼4 mm. All samples were purified by soaking in PBS at 4 °C for at least 3 d (buffer replaced daily) to remove any ROS generated during hydrogel curing. The control hydrogels without azo mechanophores were prepared similarly, with 4.8 g of PEG diacrylates, 320 mg (1.14 mmol) of ACVA, and 160 mg (1.16 mmol) of K_2CO_3 dissolved in 24 mL PBS followed by curing, cutting, and purification under the same condition. Because ACVA is a small molecule, the azo group did not incorporate into the polymer and was removed during purification.

HIFU Setup for MDT. Having determined beam characteristics, including full width at half-maximum beamwidth (B_W) and depth of field (Z_F), etc., a CW HIFU triggering system was developed (Fig. 2*B* and *SI Appendix*, *SI Materials and Methods*). A mechanical irradiation of the mechanophore hydrogels could be interfered by coupling with water. To prevent this, we considered the use of a cone-shaped water container assembled with an HIFU transducer (Fig. 2*B*). The interface between water and the samples was completely sealed with an acoustic membrane. This ensures no changes in the mechanical properties of PEG hydrogels due to the contact with water. The geometry of this assembly was designed to locate the focal spot ∼2 mm away from the acoustic membrane (Fig. 2*B*), making the focal spot located at half the thickness of the sample. In addition, a 550-kHz HIFU transducer (f number of 1.4) was selected based upon the ratio of the beamwidth at the focal spot (∼3.8 mm) to the sample diameter (16 mm). This configuration enabled the most efficient stress development for the mechanophore activation in the PEG hydrogel network. It is worthwhile to note that although the boundary-reflected waves caused by the limited sample size would cause a standing wave in the sample and make it difficult to estimate the actual radiation force applied to the mechanophore particles, this would facilitate the mechanophore activation and thus, the ROS generation (44). The entire HIFU setup was controlled using a custom LabVIEW program on a personal computer (*SI Appendix*, Fig. S6), capable of temporal control of the sonication time and the input parameters. We first considered the conversion of output voltage of the beam (at the focal spot) to the acoustic pressure using a calibrated hydrophone (sensitivity of 96.00 mV·MPa^{-1}; FUS Instruments) and then, the corresponding I_{SPTA} and focal distance. We then determined the range of sonication time (10 s on, 20 s off; four cycles per spot) and I_{SPTA} (115 W·cm^{-2}) after the observation of no visible damage on the surface. We also confirmed noticeable surface damage at I_{STPA} above 135 W·cm^{-2} with characteristics of thermal damage. To achieve an optimum transfer of mechanical energy, five different sonication spots were considered (Fig. 2*B*). As described in Fig. 2*B*, the center of a sample was mounted on the membrane of the HIFU assembly, and then, the position of sample was changed along the horizontal direction for five different focal spots. A portable laser device placed over the sample was employed to achieve a better alignment between the HIFU assembly and samples (*SI Appendix*, Fig. S3).

In Vitro MDT Challenge Assay. B16F10 mouse skin melanoma cells were maintained in DMEM (Gibco) supplemented with 10% fetal bovine serum (FBS; Corning), penicillin, and streptomycin (Thermo Fisher). B16F10 cells were a gift from Edward Roy, the University of Illinois at Urbana–Champaign, Urbana, IL. E0771 mouse breast cancer cells (CH3 BioSystems) were maintained in RPMI-1640 (Gibco) supplemented with 10% FBS (Corning), penicillin, and streptomycin (Thermo Fisher). For FR challenge experiments, 0.05% trypsin-dissociated cells were counted, and 1×10^4 cells per well were seeded in cell culture–treated six-well plates (Thermo Fisher) 24 h before the start of the experiment. After sonication, the mechanophore-containing hydrogels were placed in 100-μm mesh cell strainers (Thermo Fisher) and inserted into the six wells to be completely submerged in culture media. For H_2O_2-positive controls, 9.8 M H_2O_2 solution (Sigma) was diluted in cell culture–grade H_2O (Gibco) to 10 mM stock and further diluted to working concentrations in culture media. Cells were then incubated up to 72 h without media change and counted every 24 h. For cell counting, a 4×4 grid on the plate cover was used for consistent counting fields. Cell strainers containing hydrogels and conditioned media were removed and replaced by Calcein-AM (1 μg/mL; Invitrogen) dissolved in PBS (Gibco), followed by 10 min of incubation at 37 °C. Staining solution was then replaced by PBS, and the cells were imaged on an Olympus inverted fluorescence microscope with 4× objective and the fluorescein isothiocyanate filter set. Following imaging, conditioned media and strainer containing hydrogels were replaced, and the cells were returned to the incubator. Cells were maintained at 37 °C in a 5% CO_2 incubator. Live cells positively stained by Calcein-AM were counted using FIJI (NIH) and averaged over four counting fields per well at each time point (*SI Appendix*, Fig. S7). For each image, only the green channel was analyzed. Sizing thresholds were set specific to each sample with the aim of accurately counting each individual cell, resulting in threshold ranges from (0 to 60) to (0 to 170) for melanoma B16F10 cells and from (0 to 40) to (0 to 120) for breast cancer E0771 cells. The images were then transformed into a binary image with the watershed property applied, producing an image with a black background and white cells. Using "Analyze Particles," the distinct white areas from size 20 (to exclude small artifacts and debris) to size infinity were counted. Cell counts were then compiled and analyzed in Microsoft Excel.

Tumor Cell Lines. Use of tumor cell lines has been approved by the Institutional Animal Care and Use Committee at the University of Illinois at Urbana–Champaign and adheres to guidelines and regulations from the NIH and the US Department of Agriculture.

Data Availability. All study data are included in the article and/or supporting information.

ACKNOWLEDGMENTS. G.K. and Q.W. thank Jia En Aw for the support on infrared camera measurements and the Bioacoustics Research Laboratory and the Autonomous Materials System Group in the Beckman Institute for Advanced Science and Technology at the University of Illinois at Urbana–Champaign for technical support. G.K. and J.L.C. thank Dr. Robert L. Z. Reed for discussion and technical support. We acknowledge technical support from FUS Instruments Inc. (Toronto, Canada), which made this research possible. This work is supported by NIH Grant 5R01CA184091; the Planning Grant of the Cancer Center at Illinois,; US Department of Energy, Office of Basic Energy Sciences, Division of Materials Sciences and Engineering Award DE-FG02-07ER46471 (to Q.W.); and the 2020 Research Fund (1.200116.01) of Ulsan National Institute of Science & Technology.

1. J. Li, C. Nagamani, J. S. Moore, Polymer mechanochemistry: From destructive to productive. *Acc. Chem. Res.* **48**, 2181–2190 (2015).
2. D. A. Davis *et al.*, Force-induced activation of covalent bonds in mechanoresponsive polymeric materials. *Nature* **459**, 68–72 (2009).
3. D. C. Church, G. I. Peterson, A. J. Boydston, Comparison of mechanochemical chain scission rates for linear versus three-arm star polymers in strong acoustic fields. *ACS Macro Lett.* **3**, 648–651 (2014).
4. Y. Sagara *et al.*, Rotaxanes as mechanochromic fluorescent force transducers in polymers. *J. Am. Chem. Soc.* **140**, 1584–1587 (2018).
5. Y. Chen *et al.*, Mechanically induced chemiluminescence from polymers incorporating a 1,2-dioxetane unit in the main chain. *Nat. Chem.* **4**, 559–562 (2012).
6. Z. Chen *et al.*, Mechanochemical unzipping of insulating polyladderene to semiconducting polyacetylene. *Science* **357**, 475–479 (2017).
7. C. E. Diesendruck *et al.*, Proton-coupled mechanochemical transduction: A mechanogenerated acid. *J. Am. Chem. Soc.* **134**, 12446–12449 (2012).
8. A. Piermattei, S. Karthikeyan, R. P. Sijbesma, Activating catalysts with mechanical force. *Nat. Chem.* **1**, 133–137 (2009).
9. P. Michael, W. H. Binder, A mechanochemically triggered "click" catalyst. *Angew. Chem. Int. Ed. Engl.* **54**, 13918–13922 (2015).
10. M. B. Larsen, A. J. Boydston, "Flex-activated" mechanophores: Using polymer mechanochemistry to direct bond bending activation. *J. Am. Chem. Soc.* **135**, 8189–8192 (2013).
11. K. L. Berkowski, S. L. Potisek, C. R. Hickenboth, J. S. Moore, Ultrasound-induced site-specific cleavage of azo-functionalized poly(ethylene glycol). *Macromolecules* **38**, 8975–8978 (2005).
12. R. Göstl, R. P. Sijbesma, π-extended anthracenes as sensitive probes for mechanical stress. *Chem. Sci. (Camb.)* **7**, 370–375 (2016).

13. M. Li, Q. Zhang, S. Zhu, Photo-inactive divinyl spiropyran mechanophore cross-linker for real-time stress sensing. *Polymer (Guildf.)* **99**, 521–528 (2016).
14. E. M. Nofen *et al.*, Stress-sensing thermoset polymer networks via grafted cinnamoyl/cyclobutane mechanophore units in epoxy. *Polym. Chem.* **7**, 7249–7259 (2016).
15. Y. Zhang *et al.*, Molecular damage detection in an elastomer nanocomposite with a coumarin dimer mechanophore. *Macromol. Rapid Commun.* **42**, e2000359 (2021).
16. J. M. Clough, J. van der Gucht, R. P. Sijbesma, Mechanoluminescent imaging of osmotic stress-induced damage in a glassy polymer network. *Macromolecules* **50**, 2043–2053 (2017).
17. A. R. Sulkanen *et al.*, Spatially selective and density-controlled activation of interfacial mechanophores. *J. Am. Chem. Soc.* **141**, 4080–4085 (2019).
18. C. E. Diesendruck, J. S. Moore, "Mechanophores for self-healing applications" in *Self-Healing Polymers: From Principles to Applications*, W. H. Binder, Ed. (Wiley-VCH Verlag GmbH & Co., 2013), pp. 193–214.
19. K. Seshimo *et al.*, Segmented polyurethane elastomers with mechanochromic and self-strengthening functions. *Angew. Chem. Int. Ed. Engl.* **60**, 8406–8409 (2021).
20. G. Hong *et al.*, Mechanoresponsive healable metallosupramolecular polymers. *Macromolecules* **46**, 8649–8656 (2013).
21. B. A. Versaw, T. Zeng, X. Hu, M. J. Robb, Harnessing the Power of Force: Development of Mechanophores for Molecular Release. *J. Am. Chem. Soc.* **143**, 21461–21473 (2021).
22. P. Agostinis *et al.*, Photodynamic therapy of cancer: An update. *CA Cancer J. Clin.* **61**, 250–281 (2011).
23. M. Trendowski, The promise of sonodynamic therapy. *Cancer Metastasis Rev.* **33**, 143–160 (2014).
24. D. E. J. G. J. Dolmans, D. Fukumura, R. K. Jain, Photodynamic therapy for cancer. *Nat. Rev. Cancer* **3**, 380–387 (2003).
25. C. Nathan, A. Cunningham-Bussel, Beyond oxidative stress: An immunologist's guide to reactive oxygen species. *Nat. Rev. Immunol.* **13**, 349–361 (2013).
26. P. T. Schumacker, Reactive oxygen species in cancer: A dance with the devil. *Cancer Cell* **27**, 156–157 (2015).
27. S. Mitragotri, Healing sound: The use of ultrasound in drug delivery and other therapeutic applications. *Nat. Rev. Drug Discov.* **4**, 255–260 (2005).
28. K. Bilmin, T. Kujawska, P. Grieb, Sonodynamic therapy for gliomas. Perspectives and prospects of selective sonosensitization of glioma cells. *Cells* **8**, 1428 (2019).
29. Q. Liu, X. Wang, P. Wang, L. Xiao, Q. Hao, Comparison between sonodynamic effect with protoporphyrin IX and hematoporphyrin on sarcoma 180. *Cancer Chemother. Pharmacol.* **60**, 671–680 (2007).
30. S. K. Wu, M. A. Santos, S. L. Marcus, K. Hynynen, MR-guided focused ultrasound facilitates sonodynamic therapy with 5-aminolevulinic acid in a rat glioma model. *Sci. Rep.* **9**, 10465 (2019).
31. X. Qian, Y. Zheng, Y. Chen, Micro/nanoparticle-augmented sonodynamic therapy (SDT): Breaking the depth shallow of photoactivation. *Adv. Mater.* **28**, 8097–8129 (2016).
32. I. Rosenthal, J. Z. Sostaric, P. Riesz, Sonodynamic therapy—a review of the synergistic effects of drugs and ultrasound. *Ultrason. Sonochem.* **11**, 349–363 (2004).
33. V. Choi, M. A. Rajora, G. Zheng, Activating drugs with sound: Mechanisms behind sonodynamic therapy and the role of nanomedicine. *Bioconjug. Chem.* **31**, 967–989 (2020).
34. M. Lafond, S. Yoshizawa, S. I. Umemura, Sonodynamic therapy: Advances and challenges in clinical translation. *J. Ultrasound Med.* **38**, 567–580 (2019).
35. S. Dromi *et al.*, Pulsed-high intensity focused ultrasound and low temperature-sensitive liposomes for enhanced targeted drug delivery and antitumor effect. *Clin. Cancer Res.* **13**, 2722–2727 (2007).
36. Y. Zhang, J. Yu, H. N. Bomba, Y. Zhu, Z. Gu, Mechanical force-triggered drug delivery. *Chem. Rev.* **116**, 12536–12563 (2016).
37. S. Huo *et al.*, Mechanochemical bond scission for the activation of drugs. *Nat. Chem.* **13**, 131–139 (2021).
38. G. Kim *et al.*, High-intensity focused ultrasound-induced mechanochemical transduction in synthetic elastomers. *Proc. Natl. Acad. Sci. U.S.A.* **116**, 10214–10222 (2019).
39. O. V. Rudenko, A. P. Sarvazyan, S. Y. Emelianov, Acoustic radiation force and streaming induced by focused nonlinear ultrasound in a dissipative medium. *J. Acoust. Soc. Am.* **99**, 2791–2798 (1996).
40. H. T. Baytekin, B. Baytekin, B. A. Grzybowski, Mechanoradicals created in "polymeric sponges" drive reactions in aqueous media. *Angew. Chem. Int. Ed. Engl.* **51**, 3596–3600 (2012).
41. T. Matsuda, R. Kawakami, R. Namba, T. Nakajima, J. P. Gong, Mechanoresponsive self-growing hydrogels inspired by muscle training. *Science* **363**, 504–508 (2019).
42. M. Talât-Erben, N. Önol, The reaction of 2-cyano-2-propyl free radicals with oxygen: 2-Cyano-2-propyl hydroperoxide. *Can. J. Chem.* **38**, 1154–1157 (1960).
43. N. S. Awad *et al.*, Ultrasound-responsive nanocarriers in cancer treatment: A review. *ACS Pharmacol. Transl. Sci.* **4**, 589–612 (2021).
44. A. A. Doinikov, Acoustic radiation force on a spherical particle in a viscous heat-conducting fluid. I. General formula. *J. Acoust. Soc. Am.* **101**, 713–721 (1997).